

# Spatial Variability Assessment of Mine Tailings

**Luis Vergaray-Astupina**, Georgia Institute of Technology, USA

**Jorge Macedo**, Georgia Institute of Technology, USA

## Abstract

The Global Industry Standard on Tailings Management (GISTM) promotes performance-based approaches in geotechnical assessments. Hence, characterizing the spatial variability of deposited tailings is expected to be a key input for some tailings storage facilities (TSFs); however, it has seldom been investigated. In this study, we assess the spatial variability of thickened and conventional tailings that have been deposited into the same TSF, providing a unique opportunity to investigate two tailings technologies. A dense array of 15 cone penetration tests (CPTUs) has been conducted to collect data. The results were processed using traditional and machine learning-based methods for data detrending when deriving random fields. In terms of correlation lengths, we find similar ranges for the thickened and conventional tailings and similar distributions, likely influenced by the depositional processes. In contrast, the variance in the conventional tailings is higher, which we attribute to its segregating nature.

## Introduction

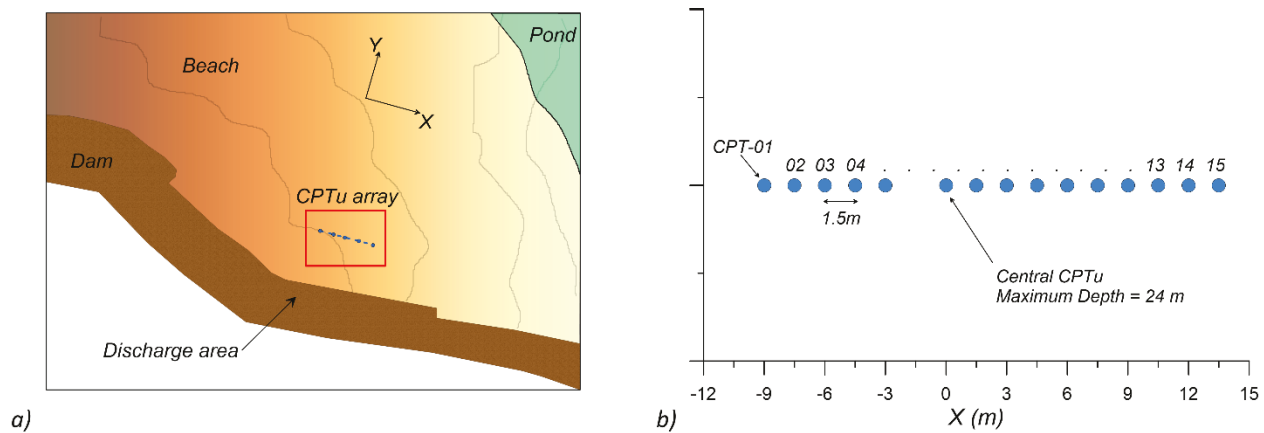
Previous efforts on characterizing the spatial variability of soil deposits have been mainly focused on natural soils, often using the random field theory (RFT). In terms of man-made waste materials, the Bagińska et al. (2016) study characterized the vertical spatial variability of a mine waste dump in a coal mine using CPTu. However, they focused only on the vertical variability due to the large spacing between the CPTUs. Regarding mine tailings, to the best of the author's knowledge, there have been no previous efforts to characterize the extent of their spatial variability at a local scale considering vertical and horizontal directions, which is one of the key contributions of our study.

Advancing the spatial variability characterization of mine tailings is a step forward to enable better treatment of uncertainties in performance-based assessments, a framework recommended in the Global Industry Standard on Tailings Management (Global Tailings Review, 2020). In addition, gaining insights into the spatial variability of mine tailings provides valuable information to improve the planning of site investigation programs for TSFs. The spatial variability assessments of this study rely on data collected on conventional and thickened tailings using a dense array of CPTUs. In addition to the traditional use of

polynomial functions in the detrending process to assess the extent of spatial variability, we highlight the significant potential of modern machine learning-based procedures for trend removal, which is a major contribution from our study. Unlike traditional polynomial functions with limited flexibility due to their fixed forms, machine learning-based methods offer greater flexibility in capturing trends in CPTu data.

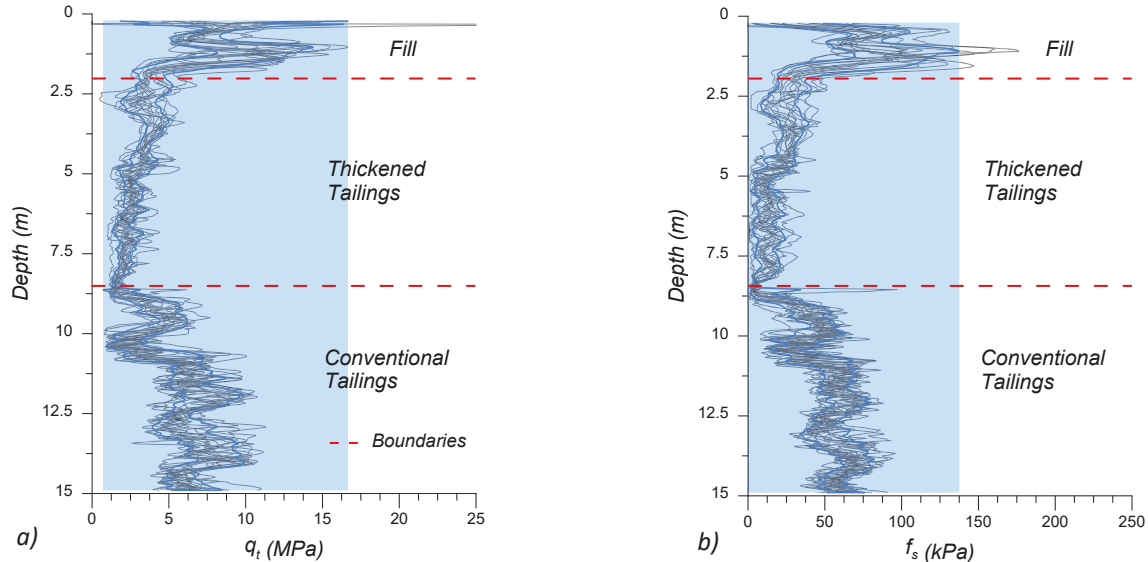
## CPTu characterization

The investigated tailings were deposited using conventional deposition starting in the 1990s until 2010, when the deposition method was changed to high-density thickened tailings, providing a unique opportunity to investigate both conventional and thickened tailings in the same TSF. The solids contents for the conventional and high-density thickened tailings are about 50% and 62 to 70% (the variation is due to seasonal change), respectively. The field characterization was planned to collect data on both tailings and included 15 CPTus. The CPTu array was oriented parallel to the discharge points in the dam, as illustrated by Figure 1a. The CPTus were conducted at a standard penetration rate of 2 cm/s and were spaced at a distance of 1.5 m, as shown in Figure 1b. The separation was selected following the recommendations of Cary (2021) to minimize any potential disturbance between nearby CPTus. The dissipation tests confirmed a phreatic surface approximately 6.1 m below the surface. The CPTus were pushed to a depth of 16 m.



**Figure 1: a) CPTu array location relative to the discharge area b) CPTu array zoom-in and labels**

Figure 2a and 2b show  $q_t$  and  $f_s$  profiles, soil layering, and the phreatic surface inferred from the CPTu tests. The inferred soil profile can be divided into three layers. The layer from the surface to 2 m is a pad access built to access the site, which is not considered in the interpretations. The second layer, extending from 2.0 to about 8.5 m, corresponds to the thickened tailings showing relatively uniform  $q_t$ ,  $f_s$ , and a linear trend in  $u_2$ . The conventional tailings underlay the thickened tailings and extend to the bottom of the profile, showing a more erratic variation of  $q_t$ ,  $f_s$  and  $u_2$  values. The separation of the conventional and thickened tailings at about 8.5 m is consistent with the tailing's deposition history.

Figure 2: a)  $q_t$ , and b)  $f_s$ , profiles

### Spatial variability assessment

The inherent spatial variability of soils can be modeled with the random field theory (RFT), which has been used in several previous studies mainly focused on natural soils. In the following, we provide a brief overview of the RFT framework and its use in assessing spatial soil variability. Interested readers can refer to Jaksa et al. (1999) and Bong and Stuedlein (2017) for additional details. Under the RFT framework, a measurement of some spatially varying soil property of interest  $g(z)$  at a given depth  $z$  can be expressed as the sum of a deterministic trend  $[t(z)]$  and a fluctuating component  $[w(z)]$  as expressed by Equation 1. The spatially varying parameter of interest is then characterized by the correlation length ( $\delta$ ), and the coefficient of variation ( $COV$ ) of  $w(z)$ .  $\delta$  is a measure of the distance within which a particular measurement is correlated, and  $COV$  is the standard deviation ( $\sigma$ ) of  $w(z)$  normalized by the mean of  $t(z)$ .

$$g(z) = t(z) + w(z) \quad (1)$$

The  $\delta$  can be calculated by different geostatistical procedures (e.g., Jaksa, 1995; Vanmarcke, 1977; DeGroot and Baecher, 1993). In particular, the use of autocorrelation models to fit the autocorrelation in the observed data is common in geotechnical applications. In this procedure, the sample autocorrelation function  $\rho(\tau_j)$  – i.e., based on the observed data, which defines the spatial correlation for a given lag distance ( $\tau_j$ ) on the measurement of interest – is evaluated according to Equation 2.

$$\rho(\tau_j) = \frac{\sum_{i=1}^{n_d-j} w_i \times w_{i+j}}{\sum_{i=1}^{n_d-j} w_i^2} \quad (2)$$

As suggested by Box and Jenkins (1970), different lag distances  $\tau_j$  can be considered by varying the sampling space ( $\Delta z$ ) for  $j = 1, 2, 3 \dots n_d/4$ , where  $n_d$  is the sample size. Once  $\rho(\tau_j)$  is assessed,  $\delta$  can be estimated by fitting different autocorrelation models (ACMs – Table 1) to  $\rho(\tau_j)$ . In using the RFT framework, it is highly beneficial to have stationarity in  $w$ , i.e., the covariance structure only depends on the distance between observations ( $\tau$ ). Thus, a key step in assessing spatial soil variability is detrending the data (i.e., removing  $t(z)$ ), ideally leading to a stationary  $w(z)$  random field.

This study used traditional polynomial and three non-parametric machine learning (ML) methods, namely, Random Forest (Breiman, 2001), Gradient Boosting Decision Tree (GBDT – Friedman, 2001), and the K-Nearest Neighbor (KNN – Peterson, 2009) for conducting the CPTu data detrending. The autocorrelation models were fitted to  $\rho(\tau_j)$  above the Bartlett's limit  $r_B = 1.96/\sqrt{n_d}$ , where  $n_d$  is the number of samples, . The fitting is considered acceptable when the coefficient of determination  $R^2$  is above 0.9 (Phoon et al., 2003).

The stationarity conditions of the detrended data were assessed using the stationarity score ( $S$ ), which is based on the Bartlett's statistic test.  $S$  is a normalized scalar quantity (bounded from  $-1$  to  $1$ ), where negative values indicate nonstationary and positive values indicate stationary.  $S$  combines the contributions from both  $R^2$  and Bartlett's statistic and can be used as a single metric to evaluate the performance of different trend functions. Further details are provided in Macedo et al. (2024).

**Table 1: Autocorrelation models and corresponding correlation length (Uzielli and Vanucchi, 2005)**

Autocorrelation model	Functional form	Correlation length
Single exponential (SNX)	$\rho(\tau) = e^{-k \tau }$	$\delta = 2/k$
Cosine exponential (CSX)	$\rho(\tau) = e^{-k \tau } \cos k\tau$	$\delta = 1/k$
Second-order Markov (SMK)	$\rho(\tau) = (1 + k \tau )e^{-k \tau }$	$\delta = 4/k$
Square exponential (SQX)	$\rho(\tau) = e^{-(kt)^2}$	$\delta = \sqrt{\pi}/k$

## Vertical correlation length

The vertical autocorrelation length ( $\delta_{wv}$ ) was calculated by fitting four different autocorrelation models (Table 1) to the sample autocorrelation functions. Figure 3 illustrates the process by showing the results obtained for the  $q_t$  profile of CPT-14 for the conventional tailings using the CSX autocorrelation model with polynomial and random forest detrending methods. The hyperparameters that produce the highest  $S$  for each method are noted in the figure titles. In this case, a polynomial function of order two was selected because it gives the highest  $S$ . However,  $S$  is negative, implying nonstationarity. In contrast, all ML-based

methods produce stationarity (Figure 3, right column). Hence, the CSX model would be discarded if only traditional polynomials were considered.

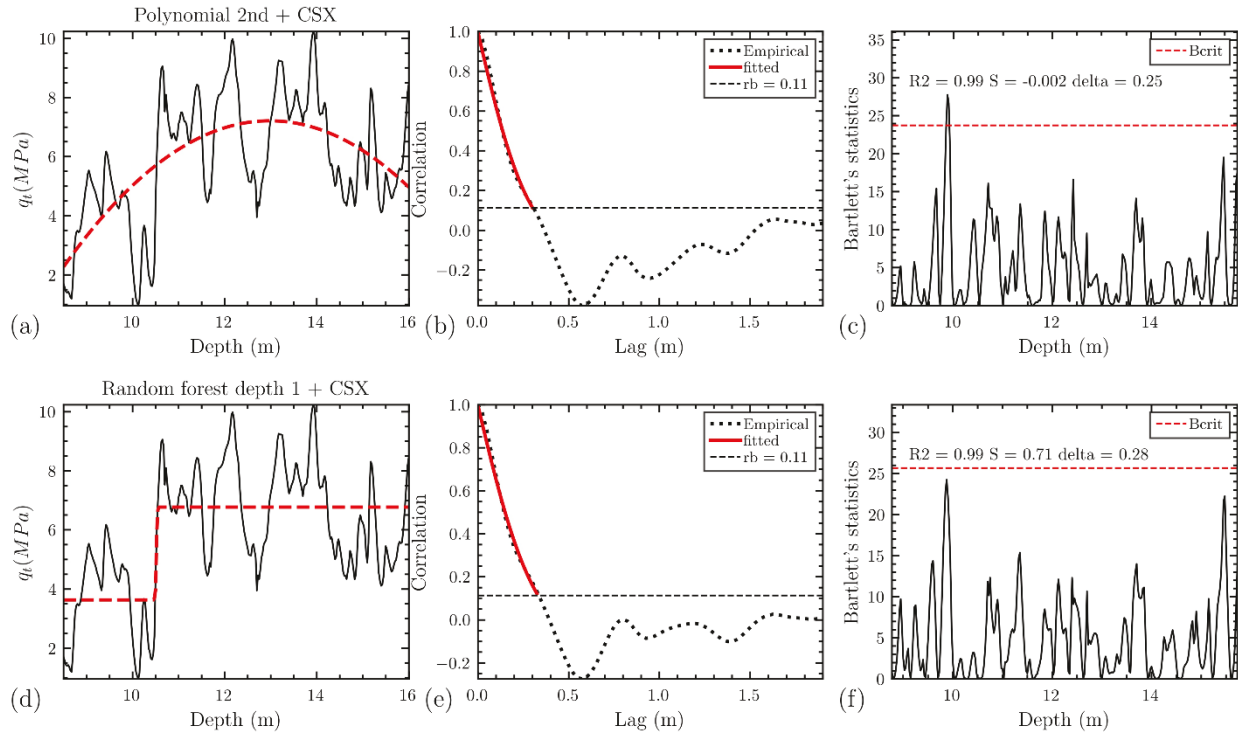


**Figure 3: Results using polynomial and ML-based trend functions for a representative  $q_t$  profile, considering the conventional tailings**

Figure 4 presents the cumulative distribution functions (CDFs) of  $\delta_{wv}$  and  $COV_{wv}$  for  $q_t$  (Figure 4a and 4b) and  $f_s$  (Figure 4c and 4d), respectively. Interestingly, the estimated  $\delta_{wv}$  and  $COV_{wv}$  values are in a relatively narrow range. In the case of the thickened tailings, the mean  $\delta_{wv}$  estimated from  $q_t$  is 0.33 m, which is smaller, but still comparable with the  $\delta_{wv}$  of 0.49 m based on  $f_s$ . In the conventional tailings, the mean  $\delta_{wv}$  estimated from  $q_t$  is 0.35 m, quite close to the mean  $\delta_{wv}$  of 0.31 m considering  $f_s$ . The  $q_t$ -based  $\delta_{wv}$  CDFs for both tailings are also consistent. The  $f_s$ -based  $\delta_{wv}$  CDFs for the thickened tailings are shifted to the right with respect to the CDFs for conventional tailings, but the  $\delta_{wv}$  are still comparable.

The similar  $\delta_{wv}$  values can be attributed to the combination of two aspects i) the deposition scheme for the conventional and thickened tailings; and ii) averaging effects in CPTu measurements. In terms of the deposition process, similar phenomena are involved in both the deposition of the conventional and thickened tailings. These phenomena include pauses in the tailings discharge (the deposition is conducted on layers), drying-wetting cycles, induced consolidation when new layers are deposited, and induced flow gradients. Moreover, even though the thickened tailings have a less segregating nature, it is still reasonable to expect some segregation under field conditions during the deposition process. In terms of the averaging

during CPTu penetration, it is well known that  $q_t$  is influenced by the response of the units that are at a distance of 1 to 3 cone diameters for soft soils and 20 to 30 cone diameters for stiffer soils (Lunne et al., 1997; Ahmadi and Robertson, 2005). Similarly,  $f_s$  also represents an averaged measurement. Thus, the relatively increased heterogeneity on the conventional tailings may have also been averaged out to some extent by the nature of the CPTu process.

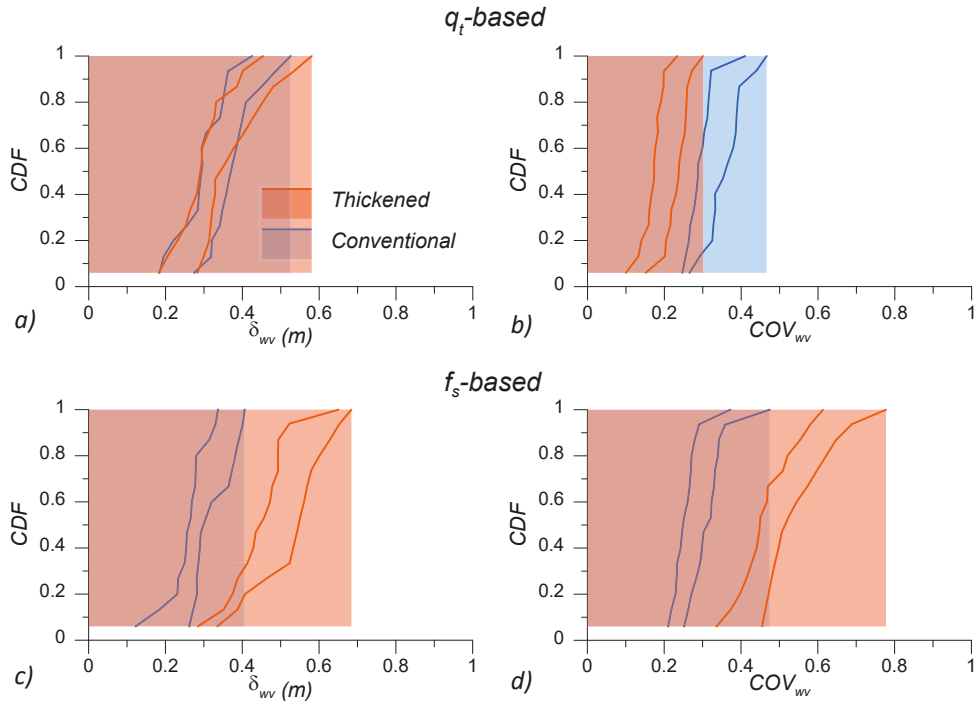


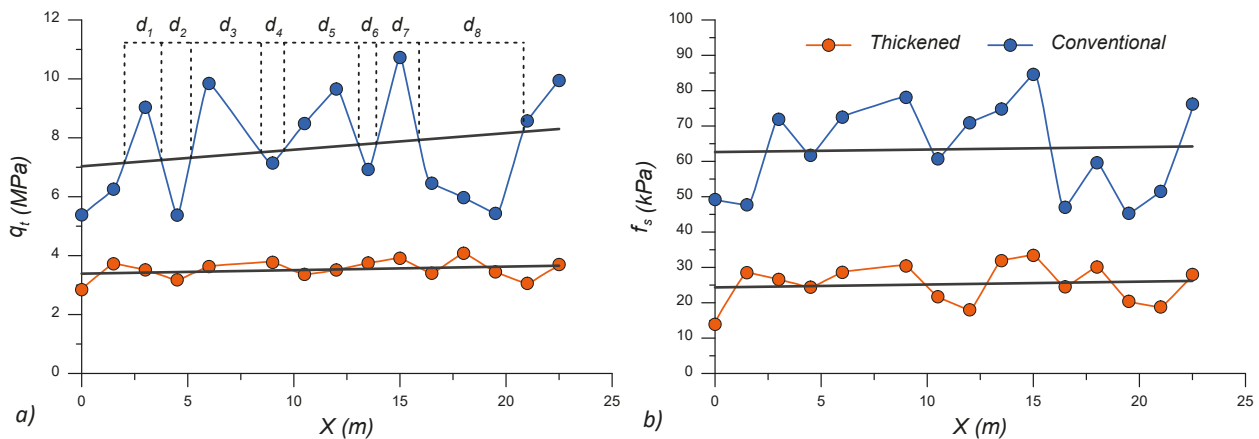
**Figure 4: Ranges of a)  $\delta_{wv}$  and b)  $COV_{wv}$  CDFs estimated from  $q_t$  data. Ranges of c)  $\delta_{wv}$  and d)  $COV_{wv}$  CDFs estimated from  $f_s$  data**

In terms of the  $COV_{wv}$  CDFs, it is important to put in context that  $COV_{wv}$  is a measurement of the fluctuation (i.e.,  $\sigma$ ) of  $w(z)$  with respect to its order of magnitude (i.e.,  $t(z)$ ). The relatively larger  $COV_{wv}$  for  $q_t$  in the conventional tailings reflects the more significant fluctuation of  $q_t$ , potentially influenced by the more segregating nature of the conventional tailings. In contrast, the larger  $COV_{wv}$  for  $f_s$  in the thickened tailings reflects the significantly lower  $f_s$  in the thickened tailings compared to the conventional tailings (i.e., a factor of about 3), which counteracts the  $\sigma$  contribution.

## Horizontal correlation length

Due to the relatively large sampling interval in the horizontal direction compared to the vertical, deriving on significantly fewer points at a given depth, the horizontal correlation length ( $\delta_{wh}$ ) is estimated following the expeditive method, which was originally proposed by Vanmarcke (1977) and has been used in previous studies for natural soils (e.g., Stuedlein et al., 2012; Bong and Stuedlein, 2017; Cary, 2021). The expeditive

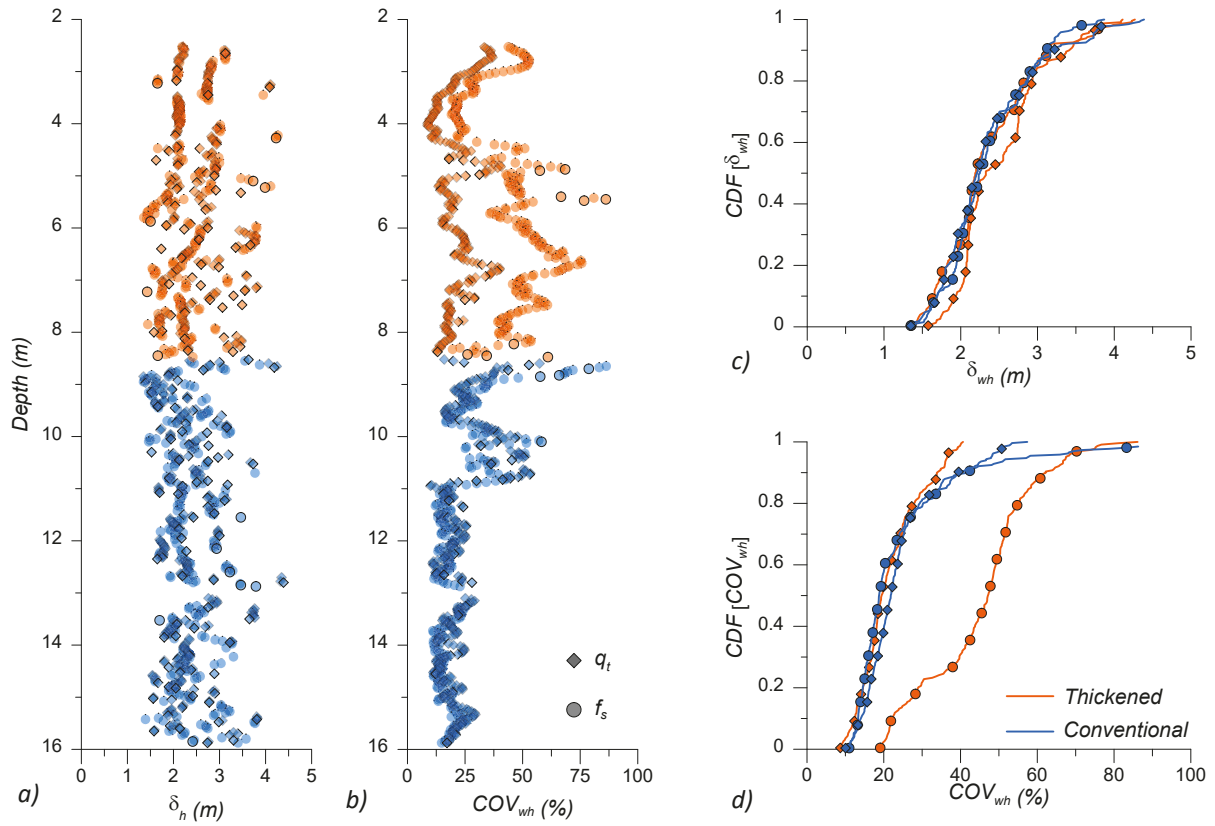
method estimates  $\delta_{wh}$  as  $\sqrt{2/\pi \bar{d}}$ , where  $\bar{d}$  is the average length of the segments obtained at the crossings of  $g(z)$  and its linear trend function  $t(z)$ , where  $g(z)$  is the metric of interest (i.e.,  $q_t$  or  $f_s$ ). Following the recommendations of Stuedlein et al. (2012) and Bong and Stuedlein (2017), in applying the expedite method, we considered a minimum of five crossings to get stable  $COV_{wh}$  and  $\delta_{wh}$  estimates. Figure 5a illustrates the  $q_t$ -based  $\delta_{wh}$  estimation in the thickened and conventional tailings at depths of 4 and 12 m, and Figure 5b illustrates the  $f_s$ -based  $\delta_{wh}$  estimation at the same depths.



**Figure 5: Application of Vanmarcke's expedite method for estimating the horizontal autocorrelation length based on a)  $q_t$  and b)  $f_s$ , considering the thickened and conventional tailings at selected depths (4 m for the thickened tailings and 12 m for the conventional tailings)**

Figure 6a shows the estimated  $\delta_{wh}$  considering  $q_t$  and  $f_s$  for the entire deposit, and Figure 6b presents the associated horizontal coefficient of variations ( $COV_{wh}$ ). It can be observed that the thickened and conventional tailings exhibit a similar  $\delta_{wh}$ . For instance, the 16 – 84 percentiles for the  $q_t$ -based  $\delta_{wh}$  is in the range of 2 to 3.5 m for the thickened tailings and in the range of 1.8 to 3.0 m for the conventional tailings. In the case of the  $f_s$ -based estimations, the 16 – 84 percentiles  $\delta_h$  is in the range of 1.7 to 3.2 m for the thickened tailings and 1.9 to 2.9 m for the conventional tailings. The similar  $\delta_{wh}$  in both tailings can be attributed to the deposition process and associated phenomena (e.g., pauses in the discharge, flow gradient, drying-wetting cycles, freezing, and consolidation) as discussed before for the  $\delta_{wv}$ .

Moreover, it is reasonable to expect segregation to have less effect in the horizontal direction compared to the vertical, which is reflected in a similar  $\delta_{wh}$ . The  $q_t$ -based  $COV_{wh}$  values tend to be slightly larger for the conventional tailings as the existing variance controls them, whereas the  $f_s$ -based  $COV_{wh}$  values are larger for the thickened tailings as they are controlled by the lower  $f_s$  values in the thickened tailings.



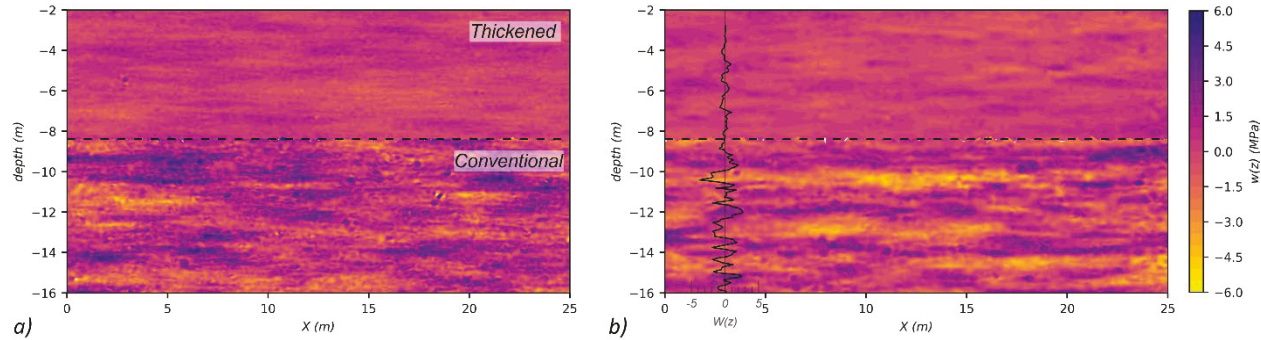
**Figure 6:** a)  $\delta_{wh}$  and b)  $COV_{wh}$  profiles based on  $q_t$  and  $f_s$ , considering the thickened and conventional tailings. CDFs of  $q_t$  and  $f_s$  based c)  $\delta_{wh}$  and d)  $COV_{wh}$  in the thickened and conventional tailings.

Figure 6c and 6d present  $q_t$ - and  $f_s$ -based CDFs for  $\delta_{wh}$  and  $COV_{wh}$ ; it can be observed that the  $\delta_{wh}$  CDFs for  $q_t$  and  $f_s$  are consistent for both the thickened and conventional tailings. In addition, similar  $q_t$ -based  $COV_{wh}$  CDFs for the thickened and conventional tailings are also observed, being also consistent with the  $f_s$ -based  $COV_{wh}$  for the conventional tailings, whereas the  $f_s$ -based  $COV_{wh}$  CDF for the thickened tailings is shifted to the right, showing larger values for reasons already discussed.

## Discussion

The generation of random fields depends on  $\delta$  and  $COV$  (or variance,  $\sigma^2$ ); hence, having similar  $\delta$ , which is the case for the thickened and conventional tailings, does not necessarily imply similar random fields. This can be illustrated by generating random fields with the parameters evaluated for the thickened and conventional tailings using the GSTools package (Muller and Schüller, 2021). Figure 7a shows one of these realizations considering the SNX autocorrelation model and parameters estimated using the GBDT model for detrending. In this case, the  $q_t$ -based estimated parameters for the thickened tailings are  $\sigma^2 = 0.3$  MPa,  $\delta_{wh} = 0.37$  m, and  $\delta_{wv} = 2.45$  m, whereas the parameters for the conventional tailings are  $\sigma^2 = 2.6$  MPa,

$\delta_{wv} = 0.41$  m, and  $\delta_{wh} = 2.29$  m. As can be inferred from these parameters, the main difference is in  $\sigma^2$ . It is interesting to note that the extent and shape of zones with similar  $w(z)$  values are comparable for the two types of tailings due to the similar  $\delta$ . However, the random field for the thickened tailings is significantly more stable (i.e., it presents less variability) due to the lower  $\sigma^2$ . Thus, despite the similar  $\delta$  for both tailings, the simulated random field for the thickened tailings shows a more homogeneous structure than conventional tailings.



**Figure 7: a) Unconditioned and b) conditioned  $q_t$ -based  $w(z)$  random field realizations for the thickened and conventional tailings**

Figure 7b presents a  $w(z)$  random field realization conditioned at various depths across the 15 CPTu locations. This conditional random field (CRF) offers a more realistic representation of spatial variability by incorporating site-specific data. Consequently, CRF realizations enhance the understanding of the distribution of tailings properties and improve the stability analysis and modeling of TSFs, which often rely on simplified assumptions, such as uniform layers, isotropic and homogeneous properties, and deterministic characteristics. By enabling probabilistic assessments, CRFs provide a more accurate and comprehensive approach to evaluating TSF stability.

## Conclusion

As the application of performance-based approaches to tailings management advances (Morgenstern, 2018), the quantification of variabilities (spatial and aleatory) is expected to become crucial, particularly for TSFs where the geotechnical characterization of mine tailings is key in assessing the overall response (e.g., the overall physical stability in upstream TSFs). In this context, we have collected data using a dense CPTu array to assess the spatial variability of two different types of tailings deposited in the same TSF. We also evaluated the potential of modern machine-learning methods for informing the estimation of random field parameters. The examined methods provided advantages, which we attribute to the interpolation nature of CPTu detrending (machine learning can act as a black box for extrapolation problems). This study's findings may prove valuable in geotechnical analyses that require adopting  $\delta$  values to account for spatial

variability in mine tailings similar to those examined in this study, specifically thickened and conventional tailings produced from gold ore. Given the lack of spatial correlation information on mine tailings, we expect that it would also be helpful as a benchmark for future efforts. Of note, case studies exist documenting the importance of spatial variability parameters for water dams (Sanchez-Lizarraga and Lai, 2014; Boulanger and Montgomery, 2016; Guo et al., 2019). Thus, it is reasonable to expect similar spatial variability studies focused on TSFs to translate into engineering practice in the future.

## Acknowledgments

This material is based upon work supported by the National Science Foundation (NSF) under Grant No. CMMI 2145092. Any opinions, findings, conclusions, or recommendations expressed in this material are those of the authors and do not necessarily reflect the views of the NSF. The PRONABEC program of the Peruvian government also provided complementary support. In addition, we would like to thank ConeTec, Newmont, and WSP-Golder for supporting the site characterization efforts. Finally, we thank Prof. Armin Stuedlein for sharing VBA codes that we used to validate our implementations and Prof. Jason DeJong for discussions when planning the CPTu campaign for the spatial variability characterization.

## References

- Ahmadi, M.M. and Robertson, P.K. 2005. Thin-layer effects on the CPT qc measurement. *Canadian Geotechnical Journal* 42(5): 1302–1317.
- Bong, T. and Stuedlein, A.W. 2017. Spatial variability of CPT parameters and silty fines in liquefiable beach sands. *Journal of Geotechnical and Geoenvironmental Engineering* 143(12).
- Boulanger, R.W. and Montgomery, J. 2016. Nonlinear deformation analyses of an embankment dam on a spatially variable liquefiable deposit. *Soil Dynamics and Earthquake Engineering* 91: 222–233.
- Box, G. and Jenkins, G. 1970 *Time Series Analysis: Forecasting and Control*. Holden-Day, San Francisco.
- Breiman, L. 2001. Random forests. *Machine Learning* 45: 5–32.
- Breysse, D., Niandou, H., Elachachi, S. and Houy, L. 2007. A generic approach to soil–structure interaction considering the effects of soil heterogeneity. *Risk and Variability in Geotechnical Engineering* 117–124.
- Cai, G., Lin, J., Liu, S. and Puppala, A.J., 2017. Characterization of spatial variability of CPTU data in a liquefaction site improved by vibro-compaction method. *KSCE Journal of Civil Engineering* 21(1): 209–219.
- Cami, B., Javankhoshdel, S., Phoon, K.-K. and Ching, J. 2020. Scale of fluctuation for spatially varying soils: Estimation methods and values. *Journal of Risk and Uncertainty in Engineering Systems, Part A: Civil Engineering* 6(4).

- Cary, J. 2021. An investigation into the role of spatial variability on liquefaction consequence severity. Master's thesis, Oregon State University.
- Ching, J., Wu, T.-J., Stuedlein, A.W. and Bong, T. 2018. Estimating horizontal scale of fluctuation with limited CPT soundings. *Geoscience Frontiers* 9(6): 1597–1608.
- DeGroot, D.J. and Baecher, G.B. 1993. Estimating autocovariance of in situ soil properties. *J. Geotech. Geoenvir. Eng.* 119(1): 147–166.
- Fenton, G.A. and Griffiths, D.V. 2005. Three-dimensional probabilistic foundation settlement. *Journal of Geotechnical and Geoenvironmental Engineering* 131(2): 232–239.
- Friedman, J. 2001. Greedy function approximation: A gradient boosting machine. *The Annals of Statistics* 29(5): 1189–1232.
- GTR (Global Tailings Review). 2020. Global Industry Standard on Tailings Management.  
[https://globaltailingsreview.org/wp-content/uploads/2020/08/global-industry-standard\\_EN.pdf](https://globaltailingsreview.org/wp-content/uploads/2020/08/global-industry-standard_EN.pdf)
- Griffiths, D.V., Fenton, G.A. and Manoharan, N. 2006. Undrained bearing capacity of two-strip footings on spatially random soil. *International Journal of Geomechanics* 6(6): 421–427.
- Guo, X., Dias, D. and Pan, Q. 2019. Probabilistic stability analysis of an embankment dam considering soil spatial variability. *Computers and Geotechnics* 113: 103093.
- Hu, Y.-G. and Ching, J. 2015. Impact of spatial variability in undrained shear strength on active lateral force in clay. *Structural Safety* 52: 121–131.
- Jaksa, M.B. 1995. The influence of spatial variability on the geotechnical design properties of a stiff, overconsolidated clay. PhD thesis, Faculty of Engineering, University of Adelaide, Adelaide, SA.
- Jaksa, M.B., Goldsworthy, J.S., Fenton, G.A., Kaggwa, W.S., Griffiths, D.V., Kuo, Y.L. and Poulos, H.G. 2005. Towards reliable and effective site investigations. *Géotechnique* 55(2): 109–121.
- Jaksa, M.B., Kaggwa, W.S. and Brooker, P.I. 1999. Experimental evaluation of the scale of fluctuation of a stiff clay. *Proceedings of the 8<sup>th</sup> International Conference on Application of Statistics and Probability*, A.A. Balkema, Rotterdam, The Netherlands, 415–422.
- Lunne, T., Robertson, P. and Powell, J. 1997. Cone penetration testing in geotechnical practice. *Soil Mechanics and Foundation Engineering* 46. 10.1007/s11204-010-9072-x.
- Müller, S. and Schüller, L. 2021. GeoStat – Framework/GSTools: v1.3.5 “Pure Pink”, Zenodo [code],  
<https://doi.org/10.5281/zenodo.5883346>
- Vergaray, L. and J. Macedo. 2024. Mechanical response of mine tailings under constant shear drained loading. *Journal of Geotechnical and Geoenvironmental engineering* 150(10): 04024082
- Peterson, L. 2009. K-nearest neighbor. *Scholarpedia* 4: 1883. 10.4249/scholarpedia.1883.

- Phoon, K.K., Quek, S.-T. and An, P. Identification of statistically homogeneous soil layers using modified bartlett statistics. *Journal of Geotechnical and Geoenvironmental Engineering* 129(7): [https://doi.org/10.1061/\(ASCE\)1090-0241\(2003\)129:7\(649\)](https://doi.org/10.1061/(ASCE)1090-0241(2003)129:7(649))
- Sanchez Lizarraga, H. and Lai, C.G. 2014. Effects of spatial variability of soil properties on the seismic response of an embankment dam. *Soil Dynamics and Earthquake Engineering* 64: 113–128.
- Stuedlein, A.W., Kramer, S.L., Arduino, P. and Holtz, R.D. 2012. Geotechnical characterization and random field modeling of desiccated clay. *J. Geotech. Geoenviron. Eng.* 1301–1313.
- Uzielli, M. and Vanucchi, G. 2005. Investigation of correlation structures and weak stationarity using the CPT soil behavior classification index. *Proceedings of the 9<sup>th</sup> International Conference on Structural Safety and Reliability – ICOSSAR 2005*, Rome.
- Vanmarcke, E.H. 1977. Probabilistic modeling of soil profiles. *Journal of the Geotechnical Engineering Division* 103(11): 1227–1246.